A Microscopic Study of the Deoxyhemoglobin-Catalyzed Generation of Nitric Oxide from Nitrite Anion†

Laura L. Perissinotti,‡ Marcelo A. Marti,‡ Fabio Doctorovich,‡ F. Javier Luque,§ and Dario A. Estrin*,‡

Departamento de Química Inorgánica, Analítica y Química Física/INQUIMAE, Facultad de Ciencias Exactas y Naturales, Universidad de Buenos Aires, Ciudad Universitaria, Pabellón II, C1428EHA Buenos Aires, Argentina, and Departament de Fisicoquímica and Institut de Biomedicina (IBUB), Facultat de Farmàcia, Universitat de Barcelona, Av. Diagonal 643, 08028 Barcelona, Spain

Received June 11, 2008; Revised Manuscript Received July 23, 2008

ABSTRACT: There is recent evidence suggesting that nitrite anion (NO_2^-) represents the major intravascular NO storage molecule whose transduction to NO is facilitated by a reduction mechanism catalyzed by deoxygenated hemoglobin (deoxy-Hb). In this work, we provide a detailed microscopic study of deoxy-Hb nitrite reductase (NIR) activity by combining classical molecular dynamics and hybrid quantum mechanical−molecular mechanical simulations. Our results point out that two alternative mechanisms could be operative and suggest that the most energetic barriers should stem from either reprotonation of the distal histidine or NO dissociation from the ferric heme. In the first proposed mechanism, which is similar to that proposed for bacterial NIRs, nitrite anion or nitrous acid coordinates to the heme through the N atom. This pathway involves HisE7 in a one or two proton transfer process, depending on whether the active species is nitrite anion or nitrous acid, to yield an intermediate Fe(III)NO species which eventually dissociates leading to NO and methemoglobin. In the second mechanism, the nitrite anion coordinates to the heme through the O atom. This pathway requires only one proton transfer from HisE7 and leads directly to the formation of a hydroxo Fe(III) complex and NO.

In the last two decades it has become apparent that nitric oxide (NO) is crucial in human physiology (*1*). Two main hypotheses about how NO is transported and stored in the bloodstream have been proposed (*1, 2*). In the first one *S*-nitrosated hemoglobin (Hb)[1] and albumin serve as storage forms of intravascular NO, and *S*-nitrosated Hb works as an allosterically regulated NO-delivery vehicle (*2, 3*). The second hypothesis proposes that the nitrite anion, which is in relative abundance in both blood and tissues, subserves this function. In blood the nitrite anion is stable compared with NO and *S*-nitrosothiols, and it can be reduced to NO by deoxygenated Hb (deoxy-Hb) (*4*). So, it seems to be an ideal storage form for NO that is conserved under normoxic conditions and employed under hypoxic conditions. The reaction of nitrite anion with deoxy-Hb may represent a source of NO bioactivity and may be the anaerobic counterpart of the oxygen-dependent production of NO by nitric oxide synthase. This adds complexity to the assumption that nitrite anion is a metabolic dead end expected to be deactivated by oxy-Hb with conversion to nitrate anion and formation of metHb.

Several studies (*5, 6*) have underscored that both deoxy-Hb and myoglobin (Mb) have nitrite reductase (NIR) activity with the capability to generate NO. The reaction of nitrite anion with deoxy-Hb has been proposed to occur via a complex mechanism not yet completely elucidated (*7, 8*). Doyle et al. (*9*) concluded that a second-order reaction was involved with an effective rate constant of $\sim$0.8 M^{-1} s^{-1} at 25 °C and pH 7.4 and that the major products were metHb and HbNO (eq 1). Since the reaction rate was linearly dependent on the concentration of H^+ in the pH range of 6−8, a mechanism that involves rate-limiting oxidative interaction of nitrous acid with Hb to produce NO and metHb, followed by rapid association of NO to Hb, was proposed. Nevertheless, Doyle et al. observed a final stoichiometry of 70% metHb and 30% HbNO instead of the expected 1:1 ratio observed by Brooks (*7*).

$$NO_2^- + HbFe^{2+}\ (\text{deoxy-Hb}) + H^+ \rightarrow HbFe^{3+}\ (\text{metHb}) + NO + OH^- \quad (1)$$

The NIR activity of Hb has been recently linked to its conformational state, it being larger when Hb is partially oygenated (*10, 11*). Thus, Huang et al. concluded that although the initial rate of the reaction has a first-order dependence on both nitrite anion and Hb, the kinetic profile does not fit to a second-order reaction but exhibits autocatalytic kinetics (*11*). In addition, under strictly anaerobic conditions the stoichiometry of the reaction is 1:1, but this

† This work was supported by grants from the ANPCYT (National Science Agency of Argentina), CONICET, and University of Buenos Aires to D.A.E. and from the Spanish Ministerio de Educación y Ciencia to F.J.L. (Grant CTQ2005-08797-C02-01/BQU). This study was funded by a fellowship to D.A.E. from the J. S. Guggenheim Foundation.

* Corresponding author. Phone: 54-11-4576-3368. Fax: 54-11-4576-3341. E-mail: dario@qi.fcen.uba.ar.

‡ Universidad de Buenos Aires.

§ Universitat de Barcelona.

[1] Abbreviations: NIR, nitrite reductase; Hb, human hemoglobin; deoxy-Hb, deoxy human hemoglobin; Mb, myoglobin; metHb, methemoglobin; HisE7, distal histidine; QM, quantum mechanics; QM-MM, quantum mecahnics−molecular mechanics; MD, molecular dynamics; DFT, density functional theory.

10.1021/bi801104c CCC: $40.75
Published on Web 08/22/2008

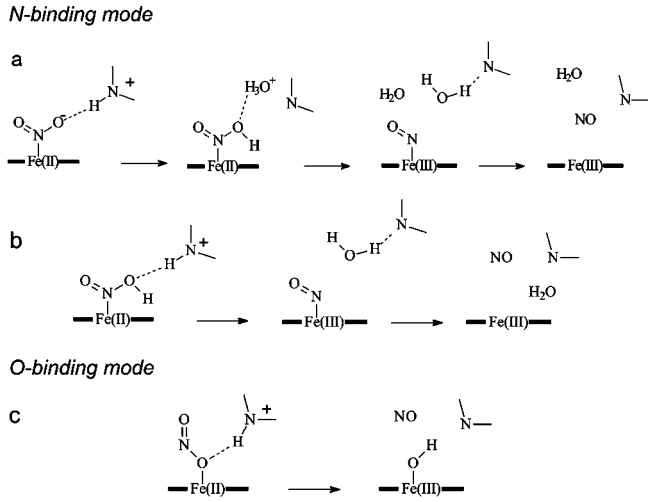

FIGURE 1: Proposed NO generation mechanisms catalyzed by Hb.

can vary significantly if there is even a slight oxygen contamination. Recently, Basu et al. (*12*) have shown that the NO produced by deoxy-Hb-catalyzed nitrite reduction may react with nitrite-bound metHb to yield N_2O_3, which may play a key role in nitrite-dependent signaling. This important finding implies that hemoglobin acts as an allosterically regulated enzyme that converts two nitrite ions into a N_2O_3 molecule. The hypothesized mechanism requires that nitrite reacts with the metHb formed (see eq 1) to generate $Hb(Fe(III))NO_2^-$, which then reacts with NO leading to the formation of N_2O_3, regenerating the catalytic HbFe(II) site (eq 2).

$$Hb(Fe(III))NO_2^- + NO \rightarrow Hb(Fe(II)) + N_2O_3 \qquad (2)$$

According to the X-ray crystallographic structures of bacterial NIRs, reduction of nitrite anion occurs via N-coordination to the ferrous heme (*13*). Protonation of nitrite would then release a water molecule, forming a weakly bound Fe(III)NO complex that subsequently decays via NO liberation (*14*). Quantum mechanics (QM) and hybrid quantum mechanics−molecular mechanics (QM-MM) calculations for *Pseudomonas aeuruginosa* NIR suggest that the proton transfer barriers are very low (*15, 16*). Then, the rate-limiting step is thought to be NO release from the d_1-heme, which is likely to occur when the d_1-heme iron is in the oxidized state (*17*). Common features in all reported X-ray structures of NIRs are two invariant histidines and a tyrosine residue in the heme distal cavity (*18*). These histidines, which are relevant for the NIR activity, are ideally located to provide the required protons and/or participate in an array of hydrogen-bonded water molecules (*19*). In contrast to bacterial NIRs, however, the distal site of Hb contains only one potential proton donor, His58 (His63) in the α (*β*) chain (Figure 2), which is surrounded by hydrophobic residues.

Among several coordination modes of nitrite anion to metals, the predominant and thermodynamically favored nitrite coordination to iron(II) porphyrins is the η^1-N mode (*20*). However, linkage isomerism may not be unlikely, and the availability of proton donors in the distal pocket may affect the balance between O-bound and N-bound isomers. Thus, even though most nitrite adducts of heme proteins or

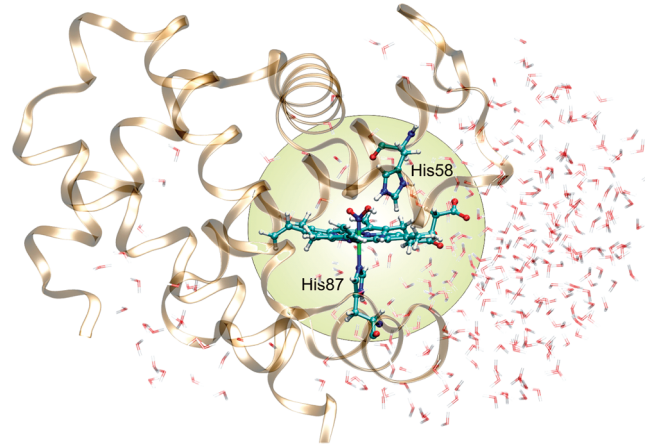

FIGURE 2: α subunit of deoxy-Hb bound to nitrous acid.

synthetic ferrous or ferric porphyrins exhibit N-coordination, an X-ray structure showing O-binding mode for ferric horse heart Mb has been recently reported (*21*). Moreover, density functional calculations in heme d_1 models and cytochrome cd_1 NIR indicate that the N-bound nitrite isomer is favored over the O-bound one by only 4.5 and 6.0 kcal/mol in the ferric and ferrous forms, respectively, which suggests that the O-bound isomer might be energetically feasible (*22*).

On the basis of the preceding considerations, different mechanisms can be proposed to account for the NIR activity of Hb. Specifically for reaction (*1*), a first one involves binding of nitrite anion through the nitrogen atom (Figure 1a). In this case, two proton transfer processes are required to remove one of the oxygen atoms of nitrite as water, which in turn can follow two schemes: (i) one proton is supplied by the histidine residue and the other comes from a solvent molecule, and (ii) the histidine supplies both protons sequentially. Alternatively, if nitrous acid (ONOH) is the bound ligand (Figure 1b), only one proton is required, and the histidine residue is ideally located to supply it. However, one should take into account that nitrous acid is relatively weak ($pK_a = 3.15$ at 298 K) (*23*) and the ratio $[ONOH]/[ONO^-]$ at pH 7 is $\sim 10^{-4}$ in aqueous solution. Finally, another potential mechanism involves O-bound nitrite coordination. In this case, only one proton is required to generate a transient coordinated nitrous acid (Figure 1c), which would release NO yielding a ferric hydroxo complex rather than the more kinetically inert iron−nitrosyl complex involved in the N-nitrite mechanism, implying that NO release would not be the rate-limiting step.

Taking into account the structural characteristics of deoxy-Hb, we undertake here a theoretical study to shed light into the binding of nitrite anion to the ferrous heme of deoxy-Hb and the feasibility of the different reaction mechanisms. Particular attention is paid to the sources of the required protons and to potential differences in reactivity between the active sites at α and *β* subunits. To this end, classical molecular dynamics (MD), QM, and QM-MM simulations are used to provide a detailed microscopic picture of the NIR reaction in deoxy-Hb.

METHODS

This study was carried out on human deoxy-Hb (PDB entry 1KD2 (*24*)) solvated with explicit water molecules. The two homodimer structure was cut, and the simulations

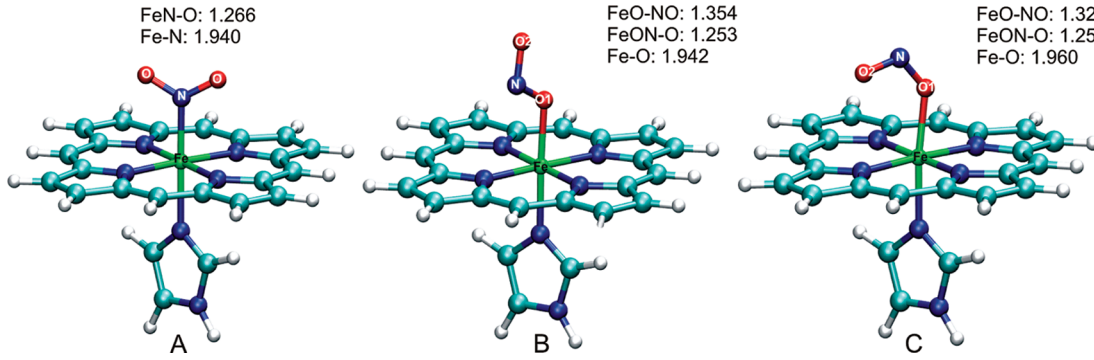

FIGURE 3: N-bound mode (A) and two O-bound modes (B and C) for nitrite anion. Distances are in Å.

were performed only for each subunit. The distal HisE7 was considered either neutral (protonated at Nε) or charged (protonated at both Nδ and Nε). The system was solvated with TIP3P (*25*) water molecules up to a distance of 30 Å from the heme center. A first step of energy minimization was performed to relax the initial structure, and then the system was heated and equilibrated at 300 K for 50 ps. The equilibrated structure was the starting point of a 10 ns MD simulation at constant temperature (300 K). SHAKE was used to keep bonds involving hydrogen atoms at their equilibrium lengths (*26*). The charges of the N- and O-coordinated nitrite anion and nitrous acid plus heme models were derived at the B3LYP/6-31G(d) using the RESP (*27, 28*) procedure. The van der Waals parameters were taken from Amber99 (*29*).

After classical optimization, QM-MM calculations were performed to explore the effect of protein and solvent environment on the nitrite reduction. The iron porphyrinate plus the ligands and selected distal (α subunit, His58; β subunit, His63) and proximal (α subunit, His87; β subunit, His92) residues were included in the quantum subsystem (shown in green in Figure 2). The rest of the protein and the water molecules were treated classically using the force field parametrization developed by Wang et al. (*29*) Only residues located less than 10 Å apart from the catalytic center were allowed to move freely. The final system consisted of 56−60 QM atoms and 15941 MM atoms. The ferrous unbound pentacoordinated heme group isolated or in the protein was treated as a high-spin quintuplet state, which is known to be the ground state for this system (*30*−*32*). The hexacoordinated N-bound and O-bound nitrite and aqueous ferric species were treated as low-spin states, since this is the ground electronic state in all cases (*30*−*32*).

The initial structure for QM-MM calculations was taken from a selected snapshot collected along the classical MD simulation. All QM computations were performed at the DFT level with the SIESTA code (*33*), which has shown a good performance for medium and large biomolecular systems and specifically for heme models (*34*). Basis functions consist of localized (numerical) pseudoatomic orbitals projected on a real space grid to compute the Hartree potential and exchange-correlation potential matrix elements. For all atoms, a double-ζ basis supplemented by polarization functions was employed, with a pseudoatomic orbital energy shift of 25 meV and a grid cutoff of 150 Ry (*33*). Calculations were performed using the generalized gradient approximation functional proposed by Perdew et al. (*35, 36*) This combination of functional, basis set and grid parameters has been validated for heme models (*15, 34, 37*). The frontier between QM and MM subsystems was treated by the scaled position link atom method adapted to our SIESTA code (*38, 39*).

Table 1: Energy Difference (kcal/mol) between N-Bound and O-Bound Coordination Modes of Nitrite Anion[a]

level of theory	$E_O - E_N$
PBE/numerical basis set (SIESTA)	10.1
PBE/SDB-ccpVDZ (Gaussian98)	5.3
BP86/DN** numerical basis set (Spartan 5.0) (22)	6.0

[a] DN**, comparable in size to 6-31G**. B3LYP/LACPV**, B3LYP/6-31G** (Jaguar or Gaussian98) ΔE, 2−3 kcal/mol.

Obtaining accurate free energy profiles requires an extensive sampling which is computationally very expensive and difficult to achieve at the DFT QM-MM level. For these reasons we computed the potential energy profile using restrained energy minimizations along the reaction path. To this end, an additional term was added to the potential energy according to $V(\zeta) = k(\zeta - \zeta_0)^2$, where k is an adjustable force constant, ζ is the reaction coordinate for the system configuration, and ζ_0 is the desired value of the reaction coordinate.

RESULTS

QM Calculations of Ligand Binding to Porphyrin. To assess the stability of N- and O-bound coordination modes of both nitrite anion and nitrous acid, the binding to a model system consisting of an iron porphyrin coordinated to imidazole was examined by QM calculations. In the case of the O-bound coordination, two different orientations of the nitrite anion were found (B and C in Figure 3), C being more stable than B by 0.9 kcal/mol. Compared to the N-bound isomer, where the N−O distance is 1.27 Å, the O-bound complex showed a longer (Fe)O1−N bond (1.32−1.35 Å) and a slightly shorter N−O2 bond (1.25 Å), which suggests increased activation toward cleavage of the O1−N bond and release of NO in this latter coordination mode (see Figure 3). Table 1 shows that the formation of the N-bound isomer is, nevertheless, favored over the O-bound one; the same result was obtained by Silaghi-Dumistrescu (*22*).

For the binding of nitrous acid, two coordination modes differing in the orientation of the O−H unit were found for the N-bound mode (Figure 4), A being more stable than B by 2.1 kcal/mol. Whereas the length of the N−O2 bond (1.22−1.23 Å) is similar to the value determined for the N-bound nitrite anion (1.27 Å; see Figure 3A), the length of the N−O1(H) bond is notably enlarged (1.43−1.44 Å vs 1.27

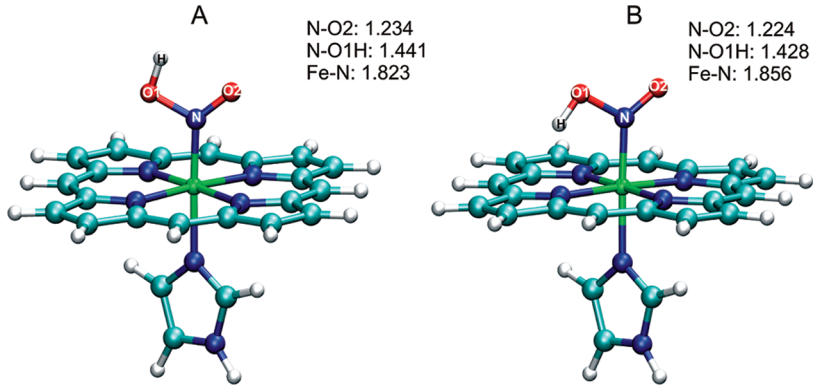

FIGURE 4: N-bound isomers for nitrous acid coordination. Distances are in Å.

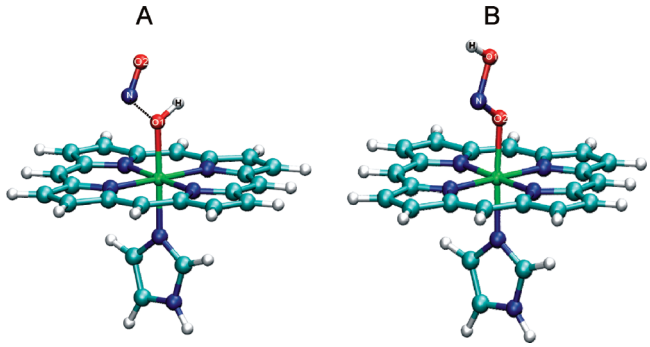

FIGURE 5: O-bound coordination modes for the nitrous acid.

Å). Accordingly, protonation of the N-bound nitrite anion enhances activation toward N−O1 bond cleavage.

If we consider the O-bound coordination of nitrous acid (i.e., the protonation of the O1 atom in the O-bound nitrite anion shown in Figure 3A), the optimized structure shows an even larger N−O1 distance (1.63 Å) and a shorter N−O2 bond length (1.20 Å) compared to the N-bound coordination mode, as was previously shown by Silaghi-Dumistrescu (*22*) (see Figure 5A). This suggests that cleavage of the N−O1 bond should occur easily leading to NO and the ferric hydroxo complex. Similar trends were found upon protonation of the other O-bound nitrite isomer depicted in Figure 3C (data not shown). Finally, another possibility consists in binding of nitrous acid through the O2 atom (or equivalently protonation of the O2 atom in the O-bound nitrite anion; see Figure 5B). In this case, the N−O1 and N−O2 bond distances of 1.42 and 1.25 Å and the structure are energetically close to that shown in Figure 5A (energy difference of 0.2 kcal/mol).

Consistently with experimental results (*40*), the N-bound mode is thermodynamically favored over the O-bound one for both nitrite anion and nitrous acid. The preference for the N-bound mode is particularly large (by 17 kcal/mol; see Supporting Information) for the nitrous acid. However, given the relatively small energy difference found for the nitrite anion (see Table 1), the protein environment might alter the preference between N- and O-coordinated structures and make the O-bound mode of nitrite anion operative in the protein.

Structural Features of Nitrite Binding to Deoxy-Hb. Based on the preceding findings, a series of 10 ns MD simulations were performed for the α and β subunits of deoxy-Hb coordinated to nitrite anion (bound through either N or O atoms) or nitrous acid (bound through the N atom). In most NIRs it is commonly accepted that the two histidines present in the active site are charged when nitrite coordinates to the enzyme. In Hb, however, there is only one distal histidine (E7) surrounded by hydrophobic residues in the heme binding site. Since protonation of HisE7 might be crucial for the NIR activity of Hb, MD simulations were performed for the neutral (with a hydrogen attached to Nϵ) and protonated states. In all cases stable trajectories were obtained, as noted by inspection of the time dependence of both the potential energy and positional root mean square deviation (see Supporting Information). Moreover, the structural features of the bound ligand showed that the interaction is more favorable when HisE7 is protonated. Therefore, for the sake of brevity we will limit ourselves to discuss the results for this latter situation, as similar trends were found for the coordination with neutral HisE7.

For the N-bound coordination of nitrite anion in the α subunit, His58 interacts alternatively with O1 or O2. The O1···H(Nϵ) or O2···H(Nϵ) distances span a broader range compared to the values found for the O-binding mode (Figure 6), where the nitrite anion adopts the B conformation instead of the C one (see Figure 3) along the simulation, suggesting that the nitrite anion is more rigid in the O-bound mode.

In the X-ray structure of deoxy-Hb, the size of the distal pocket in the β subunit is smaller than in the α subunit, and the nitrite anion is more constrained in the heme cavity. This explains why in the N-bound mode the nitrite anion mainly interacts with the NϵH unit of His63 through O1, while only occasionally O2 becomes close to NϵH, suggesting that twisting of the nitrite anion is more hindered than in the α subunit (Figure 7). This effect is less apparent in the O-bound mode, though O1 remains slightly closer than O2 to NϵH.

The structural features obtained for the binding of nitrous acid are quite similar to those of the N-bound nitrite anion. Thus, N-bound nitrous acid twists and interacts alternatively with O1 or O2 (Figure 8). However, the O1···H(Nϵ) and O2···H(Nϵ) distances show larger fluctuations than those found for the binding of nitrite anion, as expected from the lower atomic charge of O1 in nitrous acid (−0.27 e) compared to nitrite anion (−0.46 and −0.43 e for N- and O-bound modes, respectively; see Supporting Information), thus suggesting a weaker interaction of nitrous acid with the distal histidine. In the case of the β subunit nitrous acid was not easily accommodated in the heme cavity, and the distal histidine and nearby amino acids (Phe42, Phe45, Leu28, Leu31, Leu106, Val67, and Lys66) were pushed away. Moreover, His63 does not establish hydrogen bond interac-

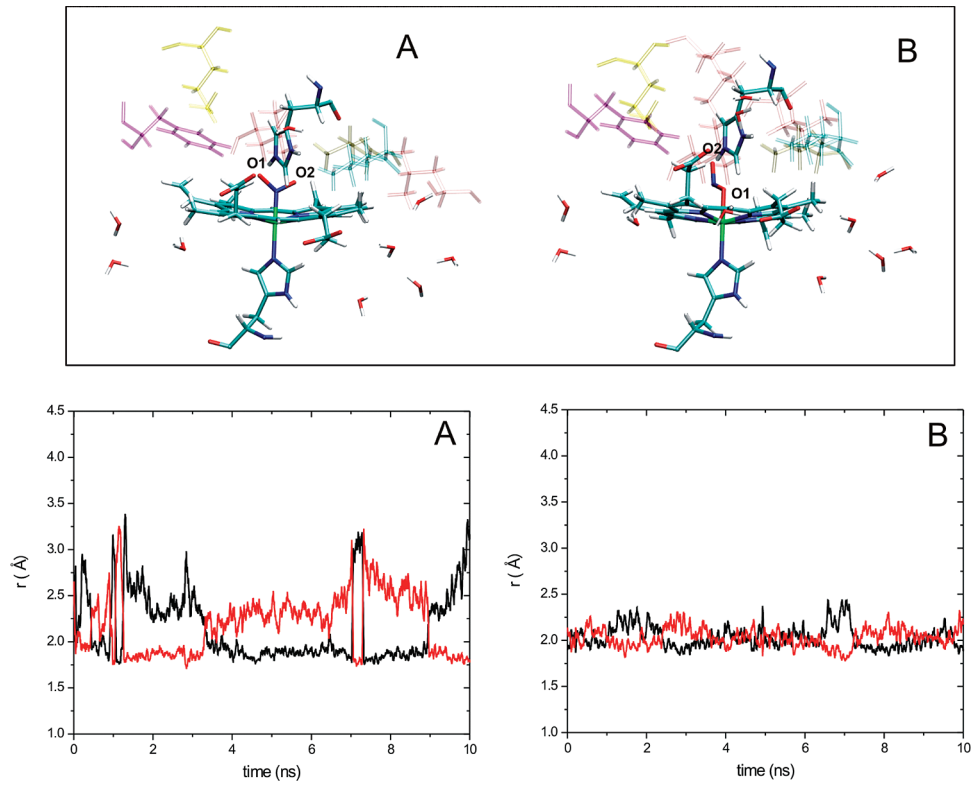

FIGURE 6: N- (A) and O-binding (B) mode of nitrite anion to the α subunit of deoxy-Hb. The nearby residues are Phe43 (violet), Met32 (yellow), Leu101 and Leu66 (pink), Val62 (ochre), and Lys61 (cyan). The O1···H(Nϵ) and O2···H(Nϵ) (His58) distances are shown in black and red, respectively.

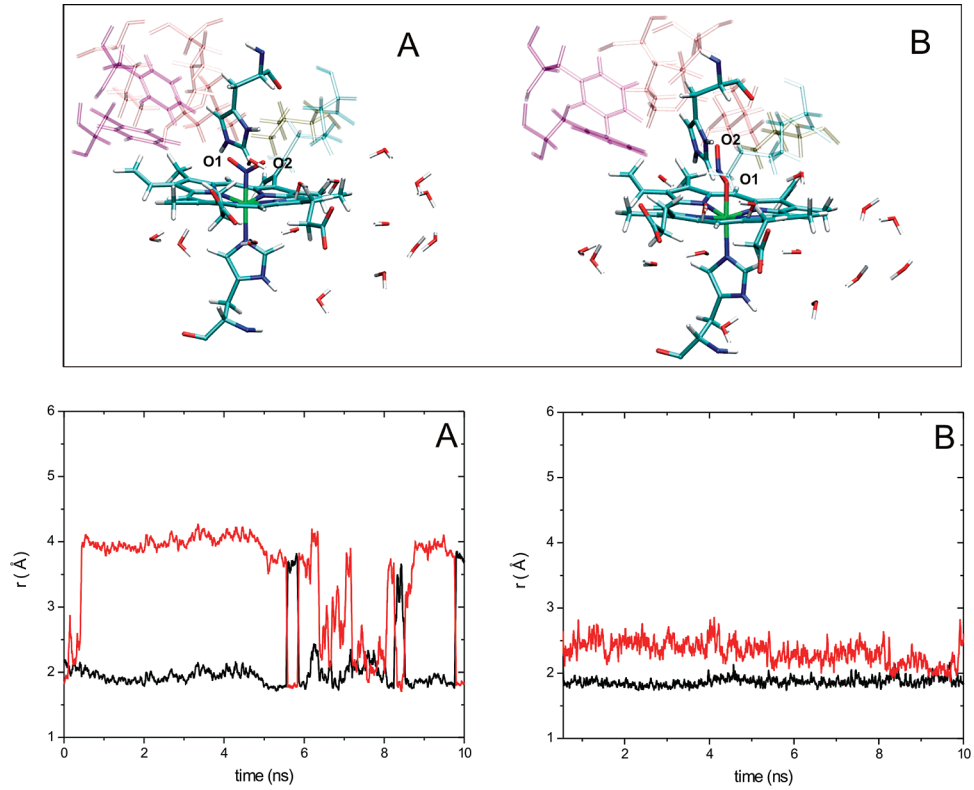

FIGURE 7: N- (A) and O-binding (B) mode of nitrite to the β subunit of deoxy-Hb. The nearby residues are Phe42 and Phe45 (violet), Leu28, Leu31, and Leu106 (pink), Val87 (ochre), and Lys66 (cyan). The O1···H(Nϵ) and O2···H(Nϵ) (His63) distances are shown in black and red, respectively.

tions with the ligand along the trajectory (the average O1···H(Nϵ) and O2···H(Nϵ) distances are 7.7 and 5.7 Å).

Taken together, the results show that in the α subunit binding of nitrite anion in both N- and O-bound modes provides stable hydrogen bond interactions with the distal HisE7 and could therefore contribute to NIR activity (see Table 2). Stable structures are also found in the binding of nitrite anion (both N- and O-bound coordination modes) to

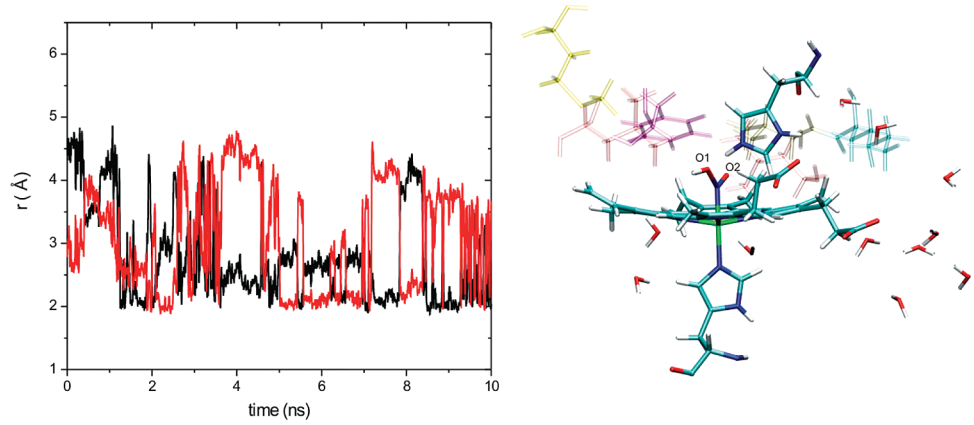

FIGURE 8: N-binding mode of nitrous acid coordinated to the α subunit of deoxy-Hb. The nearby residues are Phe42 and Phe45 (violet), Leu28, Leu31, and Leu106 (pink), Val67 (ochre), and Lys66 (cyan). The O1···H(Nϵ) and O2···H(Nϵ) (His58) distances are in black and red.

Table 2: Average Distances (Å) Extracted from 10 ns Molecular Dynamics for O1···H(Nϵ) and O2···H(Nϵ) N- and O-Binding Modes of Nitrite Anion to the α and β Subunits of Deoxy-Hb

	α subunit		β subunit	
	N-bound	O-bound	N-bound	O-bound
O1···H (His58)	2.145	2.031	2.061	1.870
O2···H (His63)	2.195	2.030	3.448	2.328

Table 3: Selected Geometrical Parameters (Å) Derived from QM-MM Geometry Optimizations for the Binding of Nitrite Anion

		N-bound nitrite		O-bound (B) nitrite		O-bound (C) nitrite	
bond distance	nitrous acid α	α	β	α	β	α	β
Fe−X[a]	1.812	1.846	1.891	2.011	1.986	2.062	2.020
O1···H (His)	2.322	1.062	1.029	1.501	1.411	1.109	1.148
N−O1	1.458	1.387	1.407	1.365	1.370	1.464	1.447
N−O2	1.225	1.236	1.233	1.245	1.248	1.203	1.210

[a] X represents O or N.

the β subunit. Nevertheless, binding of nitrous acid to the α subunit involves weaker hydrogen bond interactions with HisE7, which are even absent in the binding to the β subunit.

QM-MM Calculations of Ligand Binding to Deoxy-Hb. Selected snapshots corresponding to representative conformations were taken from the MD simulations to carry out QM-MM computations in order to explore the suitability of the mechanisms shown in Figure 1. To this end, the iron porphyrinate plus the ligand and the distal and proximal histidines were included in the quantum subsystem (Figure 2), while the rest of the protein and water molecules were treated classically. Since MD simulations showed that the interaction with the ligand was more favorable when HisE7 was charged, we will examine here the QM-MM results corresponding to this latter situation.

Ligand Affinity. The ligand affinities (ΔE_{LA}) were initially determined using an extended model composed by the heme, the ligand, and the distal and proximal histidines. Nevertheless, since a proton transfer from the distal histidine to the bound ligand was found in several cases (see below), the iron porphyrinate plus the ligand was included in the quantum subsystem, and only the distal histidine was treated classically.

$$\Delta E_{LA} = E_{\text{ligand+active site}} - (E_{\text{ligand}} + E_{\text{active site}}) \qquad (3)$$

For subunits α and β, the N-bound mode is favored over the O-bound coordination. For the binding to subunit α, the binding affinity (9.2 kcal/mol) is close to that found for the isolated system (10.1 kcal/mol; see Table 1). Nevertheless, for subunit β the O-bound coordination is destabilized by only 2.6 kcal/mol.

Proton Transfer from HisE7. QM-MM optimizations of nitrite anion coordinated to α or β subunits in the N-bound mode showed that the proton attached to His58 (α-subunit) or His63 (β-subunit) was transferred to O1, suggesting that upon binding the nitrite anion immediately acquires a proton, yielding coordinated nitrous acid. Compared to the isolated model (see Figure 4), the length of the N−O1 bond is slightly shorter (1.39 Å vs 1.44 Å; see Table 3), which reflects the H-bond interaction with HisE7. In fact, when QM-MM calculations were performed for the N-bound mode of nitrous acid, a stable intermediate was obtained, where O1 is hydrogen-bonded to HisE7 (O1···H(Nϵ) distance, 2.32 Å; see Table 3).

QM-MM optimizations were also performed for the two isomers of O-bound nitrite anion (B and C in Figure 3). For isomer C, the proton attached to HisE7 is transferred to the nitrite anion. The N−O1 bond distance is 1.46 Å (see Table 3), thus indicating the existence of an activated N−O1 breaking process. Nevertheless, the magnitude of this effect is not as large as that found for the isolated model shown in Figure 5 (the length of the N−O1 bond is 1.63 Å), and this difference likely reflects steric contraints produced by the surrounding residues, especially Met33, Leu30, Leu102, and Phe44 (α subunit) and Leu28, Leu106, and Phe42 (β subunit). In contrast, a similar proton transfer is not found for isomer B, which suggests even more unfavorable steric effects upon protonation in this coordination mode.

NO Generation in the N-Bound Coordination Mode. In order to explore the formation of NO in the case of N-bound nitrous acid, two scenarios (Figure 9), which involve the transfer of an additional proton to each of the two oxygen atoms (O1 and O2), can be envisaged. Such a proton transfer would probably occur through a mechanism that involves recovering of the protonated state of the distal histidine.

To determine the energy profile for the proton transfer to O1, the reaction coordinate $\xi = (r_2 - r_1)$ was chosen (Figure 9A). The reaction is almost barrierless (0.7 kcal/mol; see Figure 10) and leads directly to the Fe(III)NO complex and a water molecule, in agreement with the results found for

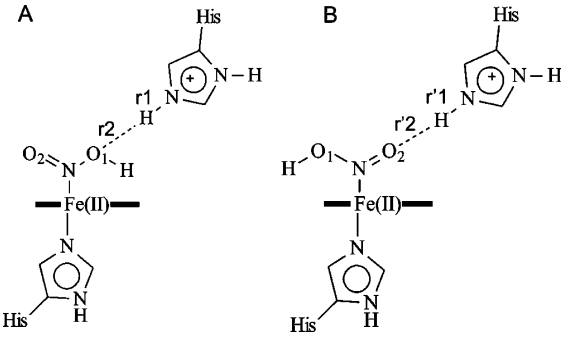

FIGURE 9: Proton transfer to O1 (A) and O2 (B).

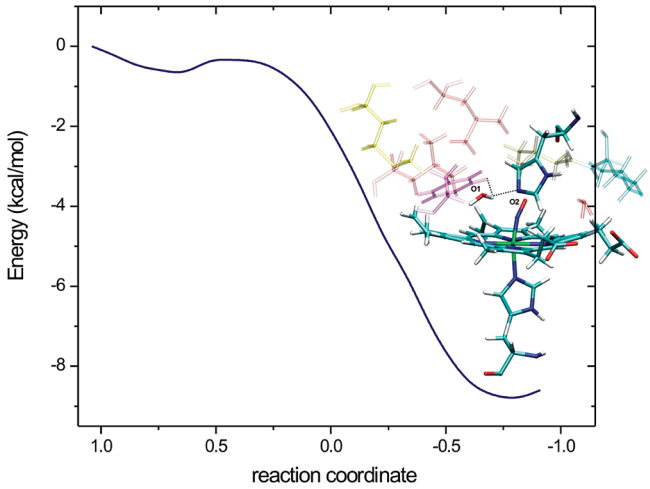

FIGURE 10: Energy profile for the proton transfer to O1 in the α subunit. The nearby residues Phe43 (violet), Met32 (yellow), Leu66 and Leu101 (pink), Val62 (ochre), and Lys61 (cyan) are shown.

Table 4: Relevant Structural Parameters (Å and deg) for Reactant and Product Species

parameter	reactant	product	free complex[a]
NO charge (e)		0.26	0.26
$Fe-N_{NO}$	1.812	1.653	1.660
$N_{NO}-O1$	1.458	2.744	
$Fe-N_{NO}-O2$	131.3	162.5	178.0
$O1-H_{58}$	2.322	0.988	
$H_{58}-N_{58}$	1.006	1.996	
$H1-O1-H_{58}$	107.1	105.5	

[a] Porphyrin Fe(III)−NO complex in vacuum.

the isolated model, where no protonated nitrous acid intermediate was detected.

The QM-MM optimized structure of the reactant conformation is shown in Figure 2, which only shows the QM system and nearby residues for the sake of clarity, and relevant geometrical parameters for the ligand and the resulting NO complex are shown in Table 4. The bound ligand was favorably oriented for the reaction with O1 hydrogen-bonded to His58. The resulting $H1-O-H_{58}$ angle (107.1°) is close to that of the water equilibrium angle. In the product state, the water molecule is located at around 2 Å from His58 and 2.6 Å from Phe44 (see Figure 10). In general, $[FeNO]^6$ compounds display linear FeNO groups in accord with predictions from the Enemark and Feltham classification (*41*). Interestingly, the angle of the product complex ($Fe-N_{NO}-O2$) is 162.5°, and the NO moiety bears a net charge of 0.26 e, thus reflecting a somewhat distorted $[FeNO]^6$ species (*42*) (compare this with 178° for the free complex in Table 4.). The results obtained here show that

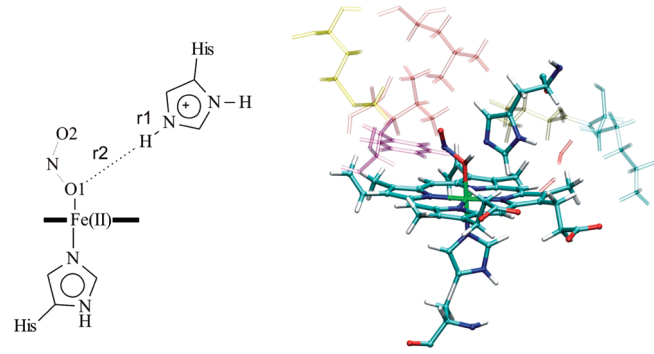

FIGURE 11: Schematic representation of the reaction coordinate used for the O-bound nitrite anion and the structure of the product state. The nearby residues Phe43 (violet), Met32 (yellow), Leu66 and Leu101 (pink), Val62 (ochre), and Lys61 (cyan) are shown.

Table 5: Relevant Structural Parameters (Å and deg) for the O-Coordinated Nitrite Anion (Isomer B and C Products) and Coordinated Nitric Oxide (Product) Enzyme Structures

	product C		product B		
bond distance (Å)	α	β	α	β	free complex
Fe−O1	2.062	1.020	2.015	1.978	1.828
N−H (His)	1.490	1.379	1.655	1.577	
O1−H (His)/O1−H	1.109	1.148	1.043	1.053	0.986
N−O1	1.464	1.447	1.481	1.457	
N−O2	1.203	1.210	1.210	1.221	

steric effects in the protein bent the NO complex, suggesting that the product cannot adopt an optimal arrangement, which might favor release of NO, in agreement with experimental results. Similar findings were observed from QM-MM calculations of nitrite reduction by NIR of *P. aeruginosa* (*15*).

Since the MD results show that most of the time O2 (i.e., the nonprotonated oxygen) is hydrogen-bonded to Nϵ*H*, we also determined the energy profile for the proton transfer to O2 using the reaction coordinate $\xi(r'_2 - r'_1)$ (see Figure 9B). The energy profile (data not shown) indicates that the reaction is not likely to occur, as the protonated nitrous acid is destabilized by at least 20 kcal/mol (similar results were found for the same process in the isolated system).

NO Generation in the O-Bound Coordination Mode. Since the O-bound nitrite anion can form a stable complex with the heme group and is energetically close to the N-bound isomer, the energy profile leading to NO generation was also examined using the reaction coordinate $\xi = (r_2 - r_1)$ (Figure 11). Even though the reaction is barrierless for both isomers B and C, the proton transfer is favored only in the case of isomer C (i.e., the protonated isomer B is 2.5 (α subunit) and 3.7 (β subunit) kcal/mol above the reactants). In addition, the product derived from the proton transfer to isomer B is disfavored by 5.5 kcal/mol relative to that formed from isomer C. The distances N−O1 and N−O2 for the product derived from the B isomer are 1.46−1.48 and 1.21−1.22 Å, which are similar to those obtained for the product derived from the C isomer (see Table 5).

DISCUSSION

When nitrite anion is bound through the N atom, it directly yields the corresponding nitrous acid adduct. After reprotonation of the distal histidine, a barrierless second proton transfer yields the ferric−NO complex and a water molecule

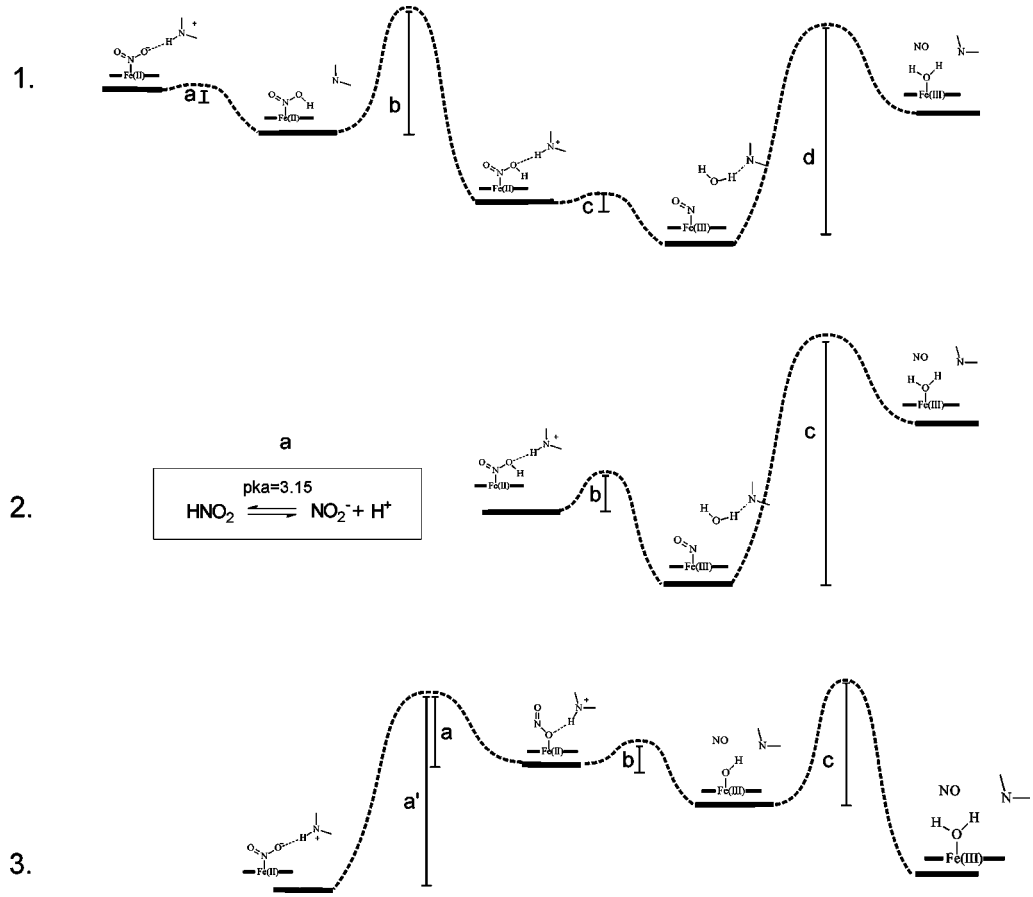

FIGURE 12: Schematic representation of the energy profile for the different mechanisms considered: (1) N-binding mode, nitrite coordination; (2) N-binding mode, nitrous acid coordination; (3) O-binding mode, nitrite coordination.

(see Figure 12 (1)). However, this mechanism opens the question about how HisE7 is reprotonated. Since neutral histidine has a pK_a of around 6.0, the population of protonated histidine at pH = 7 is ≈10%, which could limit the efficiency of the NO release. At this point, it is important to mention that the pH dependence observed by Doyle et al. could be ascribed to the reprotonation of the distal histidine. Moreover, the overall rate might also be affected by the NO eggression. Thus, Laverman et al. (*43*) measured the NO dissociation from metMb obtaining k_{off} values of 24 s^{-1} at 25 °C and a corresponding $\Delta H^{\ddagger}_{off}$ of 15.5 kcal/mol. On the basis of these considerations, the present results suggest that the most energetic barriers for the whole reaction are not associated with the chemical processes leading to the breaking of the nitrite anion, but from either reprotonation of the distal histidine or NO dissociation from the ferric heme (steps b and d in Figure 12 (1)).

Previous experimental data(*14, 44*) suggest that the only species present during the reaction of nitrite anion with T-state deoxy-Hb are deoxy-Hb, metHb, HbNO, and a metHb nitrite adduct (Hb[Fe(III)NO_2]$^{2+}$). Noticeably, MetHbNO, (Fe(II)NO^+ or Fe(III)NO), which were suggested to play a major role in this reaction, were not observed (*12*). Moreover, it is important to mention that once the first proton is transferred, the nitrous acid interacts weakly (Figure 8.) with the protonated distal histidine, and this interaction occurs mainly through the O2 atom. As mentioned before, proton transfer to O2 is not productive; in fact, the formation of the productive protonated histidine interaction with O1 could be rate-limiting.

When the nitrite anion is bound through the O atom, the reaction is barrierless in both subunits (see Figure 12 (3)). The formation of free NO and the hydroxo ferric heme seems to be not complete (see Figure 11). However, since the calculation corresponds to 0 K, thermal effects would probably facilitate NO migration across the protein, thus completing the reaction. Although our data indicate a preference for the N-bound coordination mode in both isolated models and in both α and β subunits of the protein (such a preference should be larger for the nitrous acid formed upon proton transfer according to present results for the isolated models; see above), it can be speculated that the O-bound nitrite could react immediately upon coordination (steps b and c, Figure 12 (3)) and before linkage isomerism to the N-bound nitrite occurs (step a, Figure 12 (3)). Overall, even though photoinduced linkage isomerization from coordinated N-bound to O-bound nitrite has been reported in Fe(II) porphyrins (*40, 45*), a similar process (step a′, Figure 12 (3)) in the protein environment can be ruled out. On the other hand, further support for the O-bound mechanism comes from the data of Copeland et al. (*21*), who have exposed O-bound ferric Mb crystals to dithionite for 15 s and subject a suitable crystal to crystallographic analysis. The O-bound nitrite form was retained in the presumably Fe(II) structure, but the occupancy of the ligand was reduced to 85%.

For the N-bound coordination of nitrous acid only one proton transfer is needed. The present results indicate that this process is barrierless, yielding the ferric−NO complex and a water molecule (see Figure 12 (2)). In turn, the most

Table 6: Enzyme Kinetics Derived from Michaelis−Menten Analysis for Different Kinds of Nitrite Reductases

	k_{cat} or k_2 (s^{-1})
Mb (47)	0.004
deoxy-Hb	0.005[a]
P. aeuruginosa (19)	
wild type	8
H327A or H369A	0.08

[a] Derived from Doyle et al. (9).

energetic process would be the NO dissociation from the ferric heme. However, although the nitrous acid is relatively weak ($pK_a = 3.15$ at 298 K) (*23*), the ratio [HONO]/[ONO^-] in aqueous solution at pH 7 is 10^{-4}, which strongly argues against a significant biological role of free nitrous acid in serum. Additionally, MD simulations showed that, in the case of nitrous acid binding to the β subunit, HisE7 is pushed away and no direct hydrogen bond interaction is observed, suggesting that only the binding to the α subunit can form a catalytically active complex in deoxy-Hb. Overall, the feasibility of this mechanism is questionable.

On the basis of the preceding considerations, we conclude that the most feasible mechanism involves binding of nitrite anion in the N-bound coordination mode. At this point, it is worth noting that QM-MM results support the assumption that the proton transfer processes involved in this mechanism are not rate-limiting and have low barriers. In fact, the protonation step has not been observed to be rate-limiting in neither enzymatic nor synthetic model systems for heme-based NIRs. For instance, recent results for a model of copper nitrite reductase show no significant deuterium isotope effect, confirming that the proton transfers are not rate-limiting (*46*). Moreover, the rate constant for *P. aeruginosa* is much greater than that measured for deoxy-Hb and Mb (Table 6). Interestingly, substitution of either of the two invariant histidines with alanine has a dramatic effect on nitrite reduction, and the activity resulted to be ∼1% of the wild-type enzyme (*19*). This decrease in activity likely underlies the fact that the remaining distal histidine in the mutant needs to be reprotonated in order to supply the second proton provided by the other histidine in the wild-type protein.

CONCLUSION

The present study has examined the reaction mechanism of nitrite reduction to nitric oxide catalyzed by deoxy-Hb, paying particular attention to the possibility that nitrite anion may be bonded through the N or O atom. The results point out that the most feasible mechanism involves binding of nitrite anion in the N-bound coordination mode. Even though this binding mode would require two proton transfer processes, they are not expected to be rate-limiting, and the efficiency of the enzymatic reaction might be associated with either reprotonation of the distal histidine or the increased lability of the complex formed with the reprotonated distal histidine. Binding of the nitrite anion in the O-coordination mode is predicted to be less favorable. Nevertheless, this coordination mode cannot be completely ruled out, as the single proton transfer process required for the formation of NO is found to be barrierless and could take place before linkage isomerism to the N-bound coordination mode.

Further experimental and theoretical studies should address the structural and dynamical behavior of the reprotonated distal histidine in order to assess the feasibility of the N-binding mode. The role of the R−T transition could modulate both nitrite binding and histidine reprotonation and is an interesting issue to confirm the allosteric behavior of the reaction. In addition, the issue of the catalytic production of N_2O_3 proposed by Basu et al. (*12*) will also be the subject of further mechanistic studies using computer simulation methods.

SUPPORTING INFORMATION AVAILABLE

All computed geometries, additional data, and rmsd pictures for all molecular dynamics runs are included. This material is available free of charge via the Internet at http://pubs.acs.org.

REFERENCES

1. Gladwin, M. T., and Schechter, A. N. (2004) NO contest—Nitrite versus S-nitroso-hemoglobin. *Circ. Res. 94*, 851–855.
2. Stamler, J. S., Jaraki, O., Osborne, J., Simon, D. I., Keaney, J., Vita, J., Singel, D., Valeri, C. R., and Loscalzo, J. (1992) Nitric-oxide circulates in mammalian plasma primarily as an S-nitroso adduct of serum-albumin. *Proc. Natl. Acad. Sci. U.S.A. 89*, 7674–7677.
3. Stamler, J. S., Jia, L., Eu, J. P., McMahon, T. J., Demchenko, I. T., Bonaventura, J., Gernert, K., and Piantadosi, C. A. (1997) Blood flow regulation by S-nitrosohemoglobin in the physiological oxygen gradient. *Science 276*, 2034–2037.
4. Cosby, K., Partovi, K. S., Crawford, J. H., Patel, R. P., Reiter, C. D., Martyr, S., Yang, B. K., Waclawiw, M. A., Zalos, G., Xu, X. L., Huang, K. T., Shields, H., Kim-Shapiro, D. B., Schechter, A. N., Cannon, R. O., and Gladwin, M. T. (2003) Nitrite reduction to nitric oxide by deoxyhemoglobin vasodilates the human circulation. *Nat. Med. 9*, 1498–1505.
5. Reutov, V. P. (1999) Biochemical predetermination of the NO synthase and nitrite reductase components of the nitric oxide cycle. *Biochemistry (Moscow) 64*, 528–542.
6. Reutov, V. P., and Sorokina, E. G. (1998) NO-synthase and nitrite-reductase components of nitric oxide cycle. *Biochemistry (Moscow) 63*, 874–884.
7. Brooks, C. L. (1992) Characterization of "native" apomyoglobin by molecular dynamics simulation. *J. Mol. Biol. 227*, 375–380.
8. Kim-Shapiro, D. B., Gladwin, M. T., Patel, R. P., and Hogg, N. (2005) The reaction between nitrite and hemoglobin: the role of nitrite in hemoglobin-mediated hypoxic vasodilation. *J. Inorg. Biochem. 99*, 237–246.
9. Doyle, M. P., Pickering, R. A., Deweert, T. M., Hoekstra, J. W., and Pater, D. (1981) Kinetics and mechanism of the oxidation of human deoxyhemoglobin by nitrites. *J. Biol. Chem. 256*, 2393–2398.
10. Huang, K. T., Keszler, A., Patel, N., Patel, R. P., Patel, R. P., Gladwin, M. T., Kim-Shapiro, D. B., and Hogg, N. (2005) The reaction between nitrite and deoxyhemoglobin—Reassessment of reaction kinetics and stoichiometry. *J. Biol. Chem. 280*, 31126–31131.
11. Huang, Z., Shiva, S., Kim-Shapiro, D. B., Patel, R. P., Ringwood, L. A., Irby, C. E., Huang, K. T., Ho, C., Hogg, N., Schechter, A. N., and Gladwin, M. T. (2005) Enzymatic function of hemoglobin as a nitrite reductase that produces NO under allosteric control. *J. Clin. Invest. 115*, 2099–2107.
12. Basu, S., Grubina, R., Huang, J., Conradie, J., Huang, Z., Jeffers, A., Jiang, A., He, X., Azarov, I., Seibert, R., Mehta, A., Patel, R., King, S. B., Hogg, N., Ghosh, A., Gladwin, M. T., and Kim-Shapiro, D. B. (2007) Catalytic generation of N_2O_3 by the concerted nitrite reductase and anhydrase activity of hemoglobin. *Nat. Chem. Biol. 3*, 785–794.
13. Williams, P. A., Fulop, V., Garman, E. F., Saunders, N. F. W., Ferguson, S. J., and Hajdu, J. (1997) Haem-ligand switching during catalysis in crystals of a nitrogen-cycle enzyme. *Nature 389*, 406–412.
14. George, S. J., Allen, J. W. A., Ferguson, S. J., and Thorneley, R. N. F. (2000) Time-resolved infrared spectroscopy reveals a stable ferric heme-NO intermediate in the reaction of Paracoccus pan-

totrophus cytochrome cd(1) nitrite reductase with nitrite. *J. Biol. Chem. 275*, 33231–33237.
15. Marti, M. A., Crespo, A., Bari, S. E., Doctorovich, F. A., and Estrin, D. A. (2004) QM-MM study of nitrite reduction by nitrite reductase of Pseudomonas aeruginosa. *J. Phys. Chem. B 108*, 18073–18080.
16. Ranghino, G., Scorza, E., Sjogren, T., Williams, P. A., Ricci, M., and Hajdu, J. (2000) Quantum mechanical interpretation of nitrite reduction by cytochrome cd(1) nitrite reductase from Paracoccus pantotrophus. *Biochemistry 39*, 10958–10966.
17. Rinaldo, S., Arcovito, A., Brunori, M., and Cutruzzola, F. (2007) Fast dissociation of nitric oxide from ferrous Pseudomonas aeruginosa cd1 nitrite reductase—A novel outlook on the catalytic mechanism. *J. Biol. Chem. 282*, 14761–14767.
18. Averill, B. A. (1996) Dissimilatory nitrite and nitric oxide reductases. *Chem. Rev. 96*, 2951–2964.
19. Cutruzzola, F., Brown, K., Wilson, E. K., Bellelli, A., Arese, M., Tegoni, M., Cambillau, C., and Brunori, M. (2001) The nitrite reductase from Pseudomonas aeruginosa: Essential role of two active-site histidines in the catalytic and structural properties. *Proc. Natl. Acad. Sci. U.S.A. 98*, 2232–2237.
20. Wyllie, G. R. A., and Scheidt, W. R. (2002) Solid-state structures of metalloporphyrin NOx compounds. *Chem. Rev. 102*, 1067–1089.
21. Copeland, D. M., Soares, A. S., West, A. H., and Richter-Addo, G. B. (2006) Crystal structures of the nitrite and nitric oxide complexes of horse heart myoglobin. *J. Inorg. Biochem. 100*, 1413–1425.
22. Silaghi-Dumitrescu, R. (2004) Linkage isomerism in nitrite reduction by cytochrome cd(1) nitrite reductase. *Inorg. Chem. 43*, 3715–3718.
23. Lumme, P., and Tummavuo, J. (1965) Potentiometric determination of ionization constant of nitrous acid in aqueous sodium perchlorate solutions at 25 degrees C. *Acta Chem. Scand. 19*, 617.
24. Seixas, F. A. V., De Azevedo, W. F., Jr., and Colombo, M. F. (1999) Crystallization and X-ray diffraction data analysis of human deoxyhaemoglobin A(o) fully stripped of any anions. *Acta Crystallogr., Sect D: Biol. Crystallogr. 55*, 1914–1916.
25. Jorgensen, W. L., Chandrasekhar, J., Madura, J. D., Impey, R. W., and Klein, M. L. (1983) Comparison of simple potential functions for simulating liquid water. *J. Chem. Phys. 79*, 926–935.
26. Ryckaert, J. P., Ciccotti, G., and Berendsen, H. J. C. (1977) Numerical integration of the cartesian equations of motion of a system with constraints: Molecular dynamics of n-alkanes. *J. Comput. Phys. 23*, 327–341.
27. Bayly, C. I., Cieplak, P., Cornell, W. D., and Kollman, P. A. (1993) A well-behaved electrostatic potential based method using charge restraints for deriving atomic charges: The RESP model. *J. Phys. Chem. 97*, 10269–10280.
28. Frisch, M. J., Trucks, G. W., Schlegel, H. B., Scuseria, G. E., Cheeseman, J. R., Zakrzewski, V. G., Montgomery, J. A., Jr., Stratmann, R., Burant, J., Dapprich, S., Millam, J. M., Daniels, A. D., Kudin, K. N., Strain, M. C., Farkas, O., Tomasi, J., Barone, V., Cossi, M., Cammi, R., Mennucci, B., Pomelli, C., Adamo, C., Clifford, S., Ochterski, J., Petersson, G. A., Ayala, P. Y., Cui, Q., Morokuma, K., Malick, D. K., Rabuck, A. D., Raghavachari, K., Foresman, J. B., Cioslowski, J., Ortiz, J. V., Baboul, A. G., Stefanov, B. B., Liu, G., Liashenko, A., Piskorz, P., Komaromi, I., Gomperts, R., Martin, R. L., Fox, D. J., Keith, T., Al-Laham, M. A., Peng, C. Y., Nanayakkara, A., Gonzalez, C., Challacombe, M., Gill, P. M. W., Johnson, B., Chen, W., Wong, M. W., Andres, J. L., Gonzalez, C., Head-Gordon, M., Replogle, E. S., and Pople, J. A. (1998) *Gaussian 98 Rev. A7*, Gaussian, Inc., Pittsburgh, PA.
29. Wang, J. M., Cieplak, P., and Kollman, P. A. (2000) How well does a restrained electrostatic potential (RESP) model perform in calculating conformational energies of organic and biological molecules? *J. Comput. Chem. 21*, 1049–1074.
30. Scherlis, D. A., and Estrin, D. A. (2001) Hydrogen bonding and O-2 affinity of hemoglobins. *J. Am. Chem. Soc. 123*, 8436–8437.
31. Scherlis, D. A., Marti, M. A., Ordejon, P., and Estrin, D. A. (2002) Environment effects on chemical reactivity of heme proteins. *Int. J. Quantum Chem. 90*, 1505–1514.
32. Scheidt, W. R., and Reed, C. A. (1981) Spin-state/stereochemical relationships in iron porphyrins: implications for the hemoproteins. *Chem. Rev. 81*, 543–555.
33. Soler, J. M., Artacho, E., Gale, J. D., Garcia, A., Junquera, J., Ordejon, P., and Sanchez-Portal, D. (2002) The SIESTA method for ab initio order-N materials simulation. *J. Phys.: Condens. Matter 14*, 2745–2779.
34. Marti, M. A., Crespo, A., Capece, L., Boechi, L., Bikiel, D. E., Scherlis, D. A., and Estrin, D. A. (2006) Dioxygen affinity in heme proteins investigated by computer simulation. *J. Inorg. Biochem. 100*, 761–770.
35. Perdew, J. P., Burke, K., and Ernzerhof, M. (1996) Generalized gradient approximation made simple. *Phys. Rev. Lett. 77*, 3865–3868.
36. Perdew, J. P., Burke, K., and Ernzerhof, M. (1996) Local and gradient-corrected density functionals. *ACS Symp. Ser. 629*, 453–462.
37. Marti, M. A., Scherlis, D. A., Doctorovich, F. A., Ordejon, P., and Estrin, D. A. (2003) Modulation of the NO trans effect in heme proteins: implications for the activation of soluble guanylate cyclase. *J. Biol. Inorg. Chem. 8*, 595–600.
38. Eichinger, M., Tavan, P., Hutter, J., and Parrinello, M. (1999) A hybrid method for solutes in complex solvents: Density functional theory combined with empirical force fields. *J. Chem. Phys. 110*, 10452–10467.
39. Rovira, C., Schulze, B., Eichinger, M., Evanseck, J. D., and Parrinello, M. (2001) Influence of the heme pocket conformation on the structure and vibrations of the Fe-CO bond in myoglobin: A QM/MM density functional study. *Biophys. J. 81*, 435–445.
40. Novozhilova, I. V., Coppens, P., Lee, J., Richter-Addo, G. B., and Bagley, K. A. (2006) Experimental and density functional theoretical investigations of linkage isomerism in six-coordinate {FeNO}6 iron porphyrins with axial nitrosyl and nitro ligands. *J. Am. Chem. Soc. 128*, 2093–2104.
41. Enemark, J. H., and Feltham, R. D. (1974) Principles of structure, bonding, and reactivity for metal nitrosyl complexes. *Coord. Chem. Rev. 13*, 339–406.
42. Wasser, I. M., De Vries, S., Moenne-Loccoz, P., Schroder, I., and Karlin, K. D. (2002) Nitric oxide in biological denitrification: Fe/Cu metalloenzyme and metal complex NOx redox chemistry. *Chem. Rev. 102*, 1201–1234.
43. Laverman, L. E., Wanat, A., Oszajca, J., Stochel, G., Ford, P. C., and van Eldik, R. (2001) Mechanistic studies on the reversible binding of nitric oxide to metmyoglobin. *J. Am. Chem. Soc. 123*, 285–293.
44. Luchsinger, B. P., Rich, E. N., Yan, Y., Williams, E. M., Stamler, J. S., and Singel, D. J. (2005) Assessments of the chemistry and vasodilatory activity of nitrite with hemoglobin under physiologically relevant conditions. *J. Inorg. Biochem. 99*, 912–921.
45. Coppens, P., Novozhilova, I., and Kovalevsky, A. (2002) Photoinduced linkage isomers of transition-metal nitrosyl compounds and related complexes. *Chem. Rev. 102*, 861–884.
46. Kujime, M., and Fujii, H. (2006) Spectroscopic characterization of reaction intermediates in a model for copper nitrite reductase. *Angew. Chem., Int. Ed. 45*, 1089–1092.
47. Suruga, K., Murakami, K., Taniyama, Y., Hama, T., Chida, H., Satoh, T., Yamada, S., Hakamata, W., Kawachi, R., Isogai, Y., Nishio, T., and Oku, T. (2004) A novel microperoxidase activity: methyl viologen-linked nitrite reducing activity of microperoxidase. *Biochem. Biophys. Res. Commun. 315*, 815–822.

BI801104C